

Communication

Nitrogen Dioxide Gas Sensor Based on Ag-Doped Graphene: A First-Principle Study

Qichao Li ^{1,2} , Yamin Liu ³ , Di Chen ^{1,2,*}, Jianmin Miao ^{1,2}, Xiao Zhi ⁴, Shengwei Deng ⁵, Shujing Lin ^{1,2}, Han Jin ^{1,2} and Daxiang Cui ^{1,2}

- ¹ Key Laboratory for Thin Film and Microfabrication Technology of Ministry of Education, School of Electronic Information and Electrical Engineering, Shanghai Jiao Tong University, 800 Dongchuan Road, Shanghai 200240, China; liqichao@sjtu.edu.cn (Q.L.); jmmiao@sjtu.edu.cn (J.M.); aaron.lin@sjtu.edu.cn (S.L.); jinhan10@sjtu.edu.cn (H.J.); dxcui@sjtu.edu.cn (D.C.)
 - ² Shanghai Engineering Research Center for Intelligent Diagnosis and Treatment Instrument, 800 Dongchuan Road, Shanghai 200240, China
 - ³ Shanghai Key Laboratory of Molecular Catalysis and Innovative Materials, Department of Chemistry, Fudan University, 2005 Songhu Road, Shanghai 200438, China; yamin_liu@fudan.edu.cn
 - ⁴ Institute for Personalized Medicine, School of Biomedical Engineering, Shanghai Jiao Tong University, Shanghai 200030, China; zhixiao@sjtu.edu.cn
 - ⁵ College of Chemical Engineering, Zhejiang University of Technology, Hangzhou 310014, China; swdeng@zjut.edu.cn
- * Correspondence: dchen@sjtu.edu.cn

Abstract: High-performance tracking trace amounts of NO₂ with gas sensors could be helpful in protecting human health since high levels of NO₂ may increase the risk of developing acute exacerbation of chronic obstructive pulmonary disease. Among various gas sensors, Graphene-based sensors have attracted broad attention due to their sensitivity, particularly with the addition of noble metals (e.g., Ag). Nevertheless, the internal mechanism of improving the gas sensing behavior through doping Ag is still unclear. Herein, the impact of Ag doping on the sensing properties of Graphene-based sensors is systematically analyzed via first principles. Based on the density-functional theory (DFT), the adsorption behavior of specific gases (NO₂, NH₃, H₂O, CO₂, CH₄, and C₂H₆) on Ag-doped Graphene (Ag-Gr) is calculated and compared. It is found that NO₂ shows the strongest interaction and largest Mulliken charge transfer to Ag-Gr among these studied gases, which may directly result in the highest sensitivity toward NO₂ for the Ag-Gr-based gas sensor.

Keywords: density-functional theory; gas sensing; nitrogen dioxide; graphene; single silver doping



Citation: Li, Q.; Liu, Y.; Chen, D.; Miao, J.; Zhi, X.; Deng, S.; Lin, S.; Jin, H.; Cui, D. Nitrogen Dioxide Gas Sensor Based on Ag-Doped Graphene: A First-Principle Study. *Chemosensors* **2021**, *9*, 227. <https://doi.org/10.3390/chemosensors9080227>

Academic Editor: Boris Lakard

Received: 8 July 2021

Accepted: 12 August 2021

Published: 14 August 2021

Publisher's Note: MDPI stays neutral with regard to jurisdictional claims in published maps and institutional affiliations.



Copyright: © 2021 by the authors. Licensee MDPI, Basel, Switzerland. This article is an open access article distributed under the terms and conditions of the Creative Commons Attribution (CC BY) license (<https://creativecommons.org/licenses/by/4.0/>).

1. Introduction

High-performance detecting of toxic gas molecules, such as NO₂ and NH₃, is crucial for industry application and real-time monitoring of environmental pollutants [1,2], as it is widely agreed that NO₂ can produce acid rain and have adverse effects on plant growth [3,4]. Moreover, long-term exposure to NO₂ can result in human respiratory diseases, such as bronchitis, emphysema, and asthma [5,6]. Consequently, extensive attention and research have been focusing on the development of NO₂ sensors that are based on diverse sensing materials. Over the past decade, various kinds of relevant sensitive materials were announced, which were mainly focused on metal oxide semiconductors [7], transition-metal dichalcogenides [8–10], carbon-based materials [11], and ionic liquids [12–14]. For instance, Jang et al. reported 2D NbS₂ nanosheets for selective sensing NO₂, and studied the sensing mechanisms through (density-functional theory) DFT calculations [8]. In addition, Myung et al. prepared SnO₂/ZnO heterostructure films for detecting NO₂, which presented high response performance and quick response/recovery speed [7]. Note that among the aforementioned sensing materials, graphene exhibits many attractive properties such as facile structural control, diversified synthetic methods, and exceptionally large surface

areas; graphene in particular, with its physically/chemically stable behavior is competent to endure harsh environments (for example, strong alkali/acidic conditions) [15,16]. Thus, it is believed that graphene would be a good candidate for developing high-performance NO₂ sensors.

To date, pristine and derivatives of graphene have been intensively studied, while the pristine graphene-based sensors suffered the problem of low response signals, long recovery time and poor selectivity toward NO₂, which restricted its sensing application [11,17–19]. For example, Leenaerts et al. investigated the adsorption properties of NO₂ on pristine graphene via DFT calculation, the adsorption energy is only 0.067 eV and charge transfer is $-0.099 e$, indicating that the interaction between NO₂ and pristine graphene was weak [20,21]. On the contrary, noble metal nanoparticles (NMPs) doping has proven to be a facile and effective method of improving the response performance of graphene for gas sensing [22]. Typical examples are demonstrated by Zhang et al. who used Au to modify graphene, which showed more sensitivity to H₂S and SOF₂ than pristine graphene [23]. They also carried out DFT calculations to confirm that graphene modified with Au could enhance the electrochemical reactivity of pristine graphene and activate the adsorbed gas molecules [24]. In 2019, Guha et al. reported that the response of Pt decorated and reduced graphene oxide (rGO) toward 400 ppm HCHO is 4.5 times that of bare rGO [25]. The DFT-based first-principle calculation also illustrated that Pt promoted the chemisorption of HCHO on Pt-rGO, which contributed to improving the sensing performance. In contrast to Pt-rGO, HCHO is only physically adsorbed on bare rGO. In 2020, Zeng et al. reported the simulation based on the first-principle study and demonstrated that Pd-doped graphene showed a more outstanding SO₂ adsorption performance than intrinsic graphene [26]. Compared with these frequently reported NMPs dopants (e.g., Au, Pt, Pd) [23,26,27], Ag has more potential due to its nontoxicity, antibacterial properties, high electrical/thermal conductivity, and cost-effectiveness. In our previous work [28], we have experimentally demonstrated that Ag nanoparticles modified reduced graphene oxide materials display outstanding sensing performance toward NO₂, including excellent sensitivity, fast response/recovery speed, low limit of detection (LOD), and good selectivity. Table 1 summarizes the comparison of the NO₂ sensing performance of different types of graphene-based materials in recent experimental works. Nevertheless, the internal mechanism of the improved gas sensing behavior through doping Ag is still unclear. In view of the fact that DFT has a wide range of applications in physics and chemistry, we especially studied the properties of molecules and condensed matter, such as determined the interactions of molecules in Deep Eutectic Solvents (DES) [29–32]. Herein, we theoretically illuminate the adsorption properties of NO₂ gas on Ag–Gr via the DFT. In order to reduce the simulation complexity, the graphene is doped by a single Ag atom. There are many DFT studies recently reported on metal-doped graphene, but the selectivity studies are limited [20]. Considering this circumstance, the adsorption performances for NH₃, H₂O, CO₂, and some volatile organic compounds (CH₄, C₂H₆) are also calculated to evaluate and clarify the selectivity of Ag–Gr. We anticipate that the initiatory theoretical study can provide helpful information and instructive direction on developing high-performance NO₂ sensors using noble metal-doped graphene.

Table 1. NO₂ sensing performance comparison of graphene-based materials in recent experimental works.

Sensing Materials	Detection Range (ppm)	Response (%) ^a	Response/Recovery Time (s)	LOD (ppb)	References
Ag-rGO aerogel	0.05–5	8.6 (0.08 ppm)	75/89.5	6.9	Our previous work [28]
1D rGO fiber	1–20	0.39 (20 ppm)	180/180	813	[33]
graphene nanomesh	1–10	6 (1 ppm)	900/1200	15	[34]
rGO hydrogel	1–10	3.24 (10 ppm)	600/6180	187	[35]
Cs-GO	0.18–12.2	1.5 (0.732 ppm)	240/540	90	[36]
Al-graphene	1.2–5	8 (1.2 ppm)	360/1200	-	[37]
Au-rGO	0.5–5	33 (5 ppm)	132/386	-	[38]
Si-graphene	0.018–300	21.5 (50 ppm)	126/378	18	[18]
N-rGO	0.02–0.8	11.7 (0.8 ppm)	151/10	14	[39]
SnO ₂ -rGO	14–110	11.5 (110 ppm)	480/480	2000	[40]
Co ₃ O ₄ -rGO	0.05–10	26.8 (5 ppm)	90/2400	50	[41]
MoS ₂ -Graphene	1.2–100	6.83 (5 ppm)	300/1800	1200	[42]

^a Response = $(R_g - R_a)/R_a \times 100\%$, where R_g is the resistance in NO₂; R_a is the resistance in background gas.

2. Materials and Methods

First principle calculation is implemented in the DMol3 package [43–46]. Generalized gradient approximation (GGA) with Perdew–Burke–Ernzerhof (PBE) is used. Grimme custom method for DFT-D is chosen for better describing Van der Waals functionalization [47]. DFT Semi-core Pseudopotentials is used for core treatment, and basis sets DNP with 4.4 files. Monkhorst-pack grid parameters are set as $9 \times 9 \times 1$ for calculating electronic properties. The model contains a 4×4 graphene supercell doped with an Ag atom in the middle by replacing a carbon atom. The vacuum with 2 nm spacing in the z-axis direction is adopted for minimizing the interaction of adjacent layers of graphene. Gas molecules are added more than the distance of 0.36 nm above the Ag atom. All configurations are optimized until the energy tolerance is less than 2×10^{-5} Ha. Besides, NO₂ is a paramagnetic molecule [48,49], spin polarization is carried out in the adsorption calculation of NO₂ on Ag–Gr.

The adsorption energy (E_{ad}) of gas molecules on Ag–Gr is defined as:

$$E_{ad} = E_{Ag/G + gas} - E_{Ag/G} - E_{gas} \quad (1)$$

where $E_{Ag/G + gas}$ is the total energy after gas adsorbed on the Ag–Gr, $E_{Ag/G}$ is the isolated optimized energy of Ag–Gr, and E_{gas} is the isolated optimized energy of the gas molecule.

3. Results

For the purpose of investigating the adsorption effect of gas molecules on single Ag-doped graphene, some typical gas molecules are tested. The adsorption distance (d), adsorption energy (E_{ad}), and Mulliken charge (Q) are calculated and the values are presented in Table 2. Finally, the interaction between gas molecules and Ag-doped graphene will be analyzed in detail.

Table 2. Adsorption distance, adsorption energy, and Mulliken charge of different gas molecules on Ag-doped graphene.

Gas	d (nm)	E_{ad} (eV)	Q (e)
NO ₂	0.2224 (Ag-O)	−2.209	−0.450
NH ₃	0.2295 (Ag-N)	−1.115	0.136
H ₂ O	0.2297 (Ag-O)	−0.930	0.122
CO ₂	0.2626 (Ag-O)	−0.360	0.018
CH ₄	0.2218 (Ag-H)	−0.335	0.031
C ₂ H ₆	0.2395 (Ag-H)	−0.514	0.050

After finishing the Geometry Optimization task, the optimal stable adsorption configurations of all molecules are shown in Figure 1. For NO_2 , the N atom in NO_2 is far from Ag–Gr. The adsorption distance is defined as the nearest distance of atoms between gas molecules and Ag–Gr. Thus, the adsorption distance in $\text{NO}_2/\text{Ag-Gr}$ configuration is 0.2224 nm, which is less than the Van der Waals radii ($\text{O} = 0.155$ nm, $\text{Ag} = 0.177$ nm). The adsorption energy is -2.209 eV, which is the largest value among all gas molecules, indicating strong adsorption properties. Meanwhile, the Mulliken transfer charge is -0.45 e, suggesting that the charges transfer from Ag–Gr to NO_2 , where NO_2 acts as an electron acceptor. The Mulliken charge value is also the largest compared with other gases, meaning the super electron capture capability of NO_2 . Ag–Gr is one of the p-type semiconductor materials. When NO_2 molecules as the electron acceptor are adsorbed on Ag–Gr, the resistance of Ag–Gr will dramatically decrease. The total density of states (DOS) is calculated to further study the interaction between NO_2 and Ag–Gr. As presented in Figure 2a, the DOS changes obviously after NO_2 adsorbed on Ag–Gr, especially, near both sides of the Fermi level. Thus, both the largest adsorption energy and Mulliken transfer charge with the addition of dramatic DOS change illuminate stronger interaction between NO_2 and Ag–Gr than others, which is beneficial for gas sensitivity.

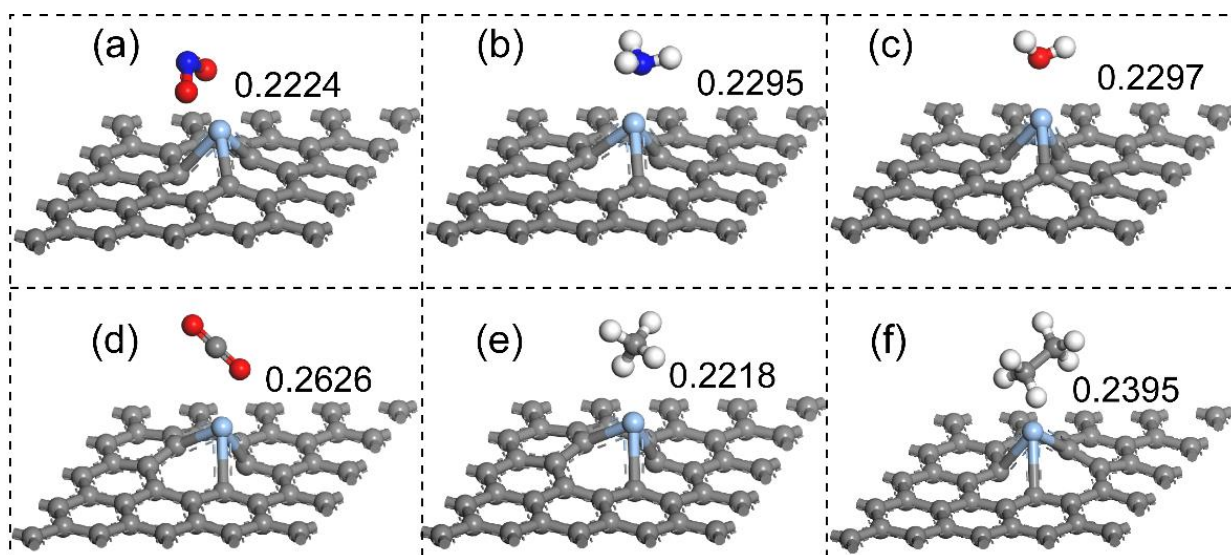


Figure 1. The optimal stable adsorption configurations of Ag–Gr with (a) NO_2 , (b) NH_3 , (c) H_2O , (d) CO_2 , (e) CH_4 , and (f) C_2H_6 .

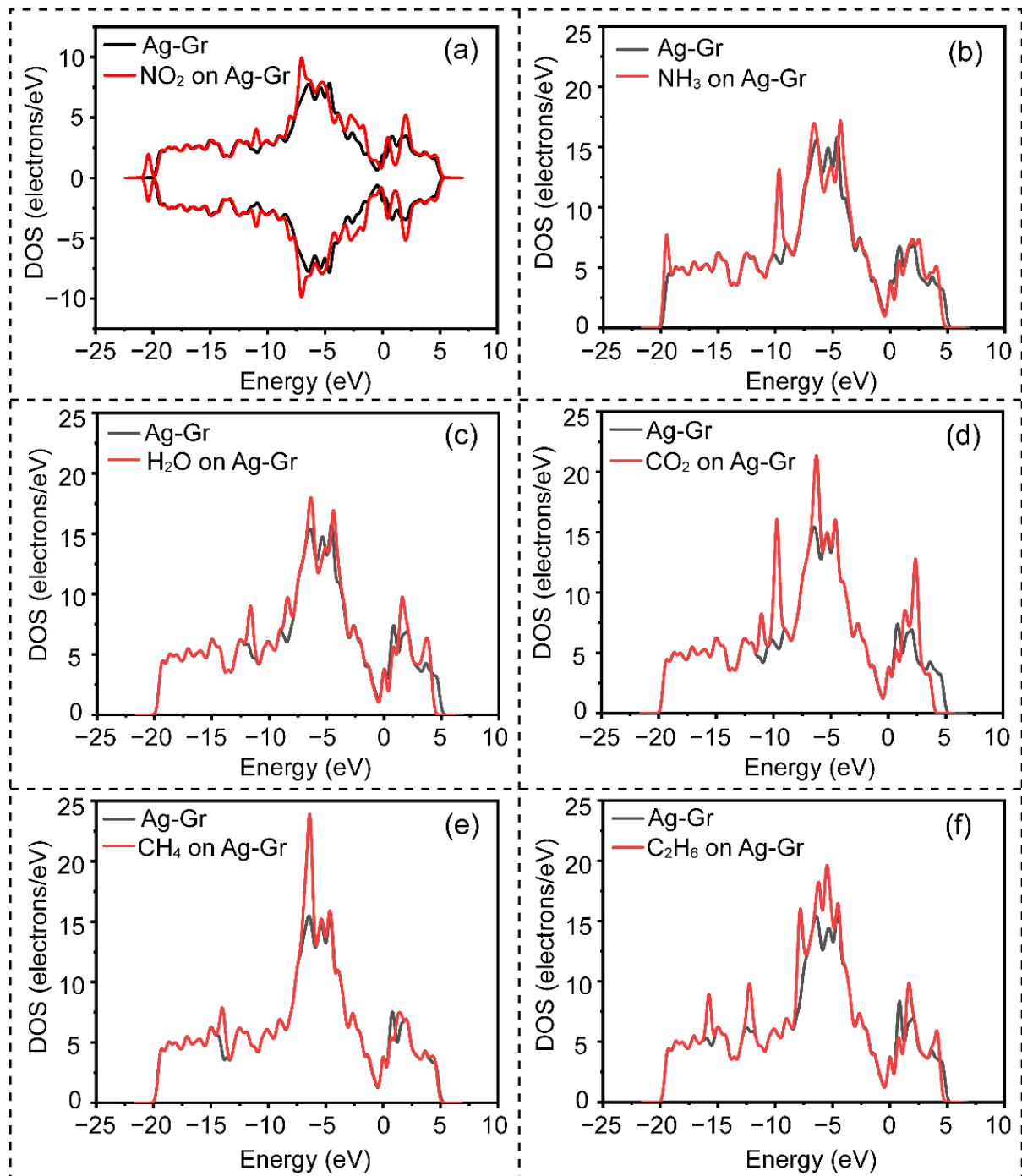


Figure 2. The DOS comparison of Ag-Gr and Ag-Gr adsorption with (a) NO₂, (b) NH₃, (c) H₂O, (d) CO₂, (e) CH₄, and (f) C₂H₆.

Many recent studies on NO₂ sensors based on graphene or graphene derivatives have reported that the sensors have a response to NH₃ [50]. Thus, the adsorption performance of NH₃ on Ag-Gr should be investigated. After calculation, the adsorption distance of NH₃ on Ag-Gr is 0.2297 nm (Figure 1b), also less than Van der Waals radii (N = 0.16 nm, Ag = 0.177 nm). The adsorption energy is -1.115 eV and the Mulliken charge is 0.136 e, which indicates that obvious interaction takes place in the adsorption process, and the charge transfers from NH₃ to Ag-Gr. Contrary to NO₂, NH₃ plays the donor role. When exposed to the NH₃ atmosphere, the resistance of p-type Ag-Gr-based gas sensors will increase. The different change direction of resistance caused by NH₃ and NO₂ can be used

for discriminating the two gas molecules. Besides, the DOS near the Fermi level has a small change (Figure 2b). Hence, NH_3 on Ag–Gr can slightly change the conductivity of Ag–Gr-based sensor.

Humidity interference in the sensing process often influences the accuracy of the gas sensors. The cross-response of humidity should be suppressed. Therefore, the adsorption properties of water on Ag–Gr are studied. The adsorption distance of H_2O on Ag–Gr is 0.2296 nm, less than Van der Waals radii ($\text{O} = 0.155$ nm, $\text{Ag} = 0.177$ nm). The adsorption energy (-0.930 eV) and Mulliken charge (0.122 e) show that the charge transfers from H_2O (donor role) to Ag–Gr. In Figure 2c, after adsorption, the contribution from H_2O electronic states to the total DOS of Ag–Gr is localized from -9.0 eV to -3.7 eV in valence bands and from 0.4 eV to 5 eV in conduction bands. Although H_2O can interact with Ag–Gr, the interaction could be weakened by some suitable methods, such as heating through a microheater, which is demonstrated as an effective method in our previous work [28].

In the case of CO_2 , the adsorption distance on Ag–Gr is 0.2626 nm. Figure 2d shows that the contribution of CO_2 electronic states to total DOS is far away from the Fermi level. The adsorption energy is -0.360 eV, and the Mulliken transfer charge is only 0.018 e. The weak charge transfer indicates that the sensor based on Ag–Gr is not sensitive to CO_2 .

For organic volatile compounds (VOCs), such as CH_4 and C_2H_6 , the adsorption distances on Ag–Gr are 0.2218 nm and 0.2395 nm, respectively. From Figure 2e–f, the contributions of CH_4 and C_2H_6 electronic levels are both far away from the Fermi level. The adsorption energy of the two gas is -0.335 eV (CH_4) and -0.514 eV (C_2H_6). The Mulliken transfer charge of C_2H_6 is only 0.050 e, indicating the weak sensitivity of Ag–Gr toward C_2H_6 . For CH_4 , both adsorption energy and Mulliken transfer charge (0.031 e) are very small, corresponding to the poor response toward CH_4 for Ag–Gr. Actually, the gas sensor based on Ag nanoparticles modified reduced graphene oxide has been experimentally demonstrated to have a poor response toward VOCs in our previous work. This characteristic allows Ag–Gr-based NO_2 sensors to have good selectivity.

The total charge densities are calculated for further investigating the interaction of gas molecules and Ag–Gr. As shown in Figure 3a, a distinct electron orbital overlap between Ag–Gr and NO_2 molecules is observed. The strong overlap is consistent with the intense interaction once the Ag–Gr-based gas sensor is exposed to the NO_2 polluted air. Additionally, the difference charge densities are also performed. Figure 4 shows the difference charge densities of gas molecules' adsorption on Ag–Gr. The colors blue and red are represented as losing electrons and obtaining electrons, respectively. As seen from Figure 4a, the conspicuous red regions surround O atoms of NO_2 , and at the same moment, the obvious blue region surrounds the Ag atom. The electrons enrichment areas around O atoms nearly contact with the core electrons area around the Ag atom. In this case, strong interaction occurs between Ag and O atoms. Consequently, adsorbed NO_2 will significantly change the electrical conductivity of Ag–Gr, resulting in outstanding sensitivity. Compared with NO_2 , the electron orbital overlap between both NH_3 and H_2O with Ag–Gr are smaller (Figure 3b–c), indicating a low sensitivity for Ag–Gr-based gas sensors. From difference charge densities plots in Figure 4b–c, we can see that the blue regions are obvious, and small red regions appear around both NH_3 and H_2O molecules. This is due to the donor properties of these two types of molecules. As for CO_2 and VOCs, shown in Figure 3d–f, it is noted that no electron orbital overlap exists between the other three gases (CO_2 , CH_4 , and C_2H_6) with Ag–Gr, demonstrating that the adsorption of CO_2 , CH_4 , and C_2H_6 on Ag–Gr layers are physisorption, resulting in the facts of very few charges transferring between gas molecules and Ag–Gr. This could be one of the main reasons that an Ag–Gr-based gas sensor is not sensitive to VOCs. From the six inserts of deformation electron density isosurfaces in Figure 3, we can also obtain consistent results, because the electron accumulation (pink) and depletion (yellow) regions between NO_2 and Ag are more obvious than those between other gas molecules and Ag.

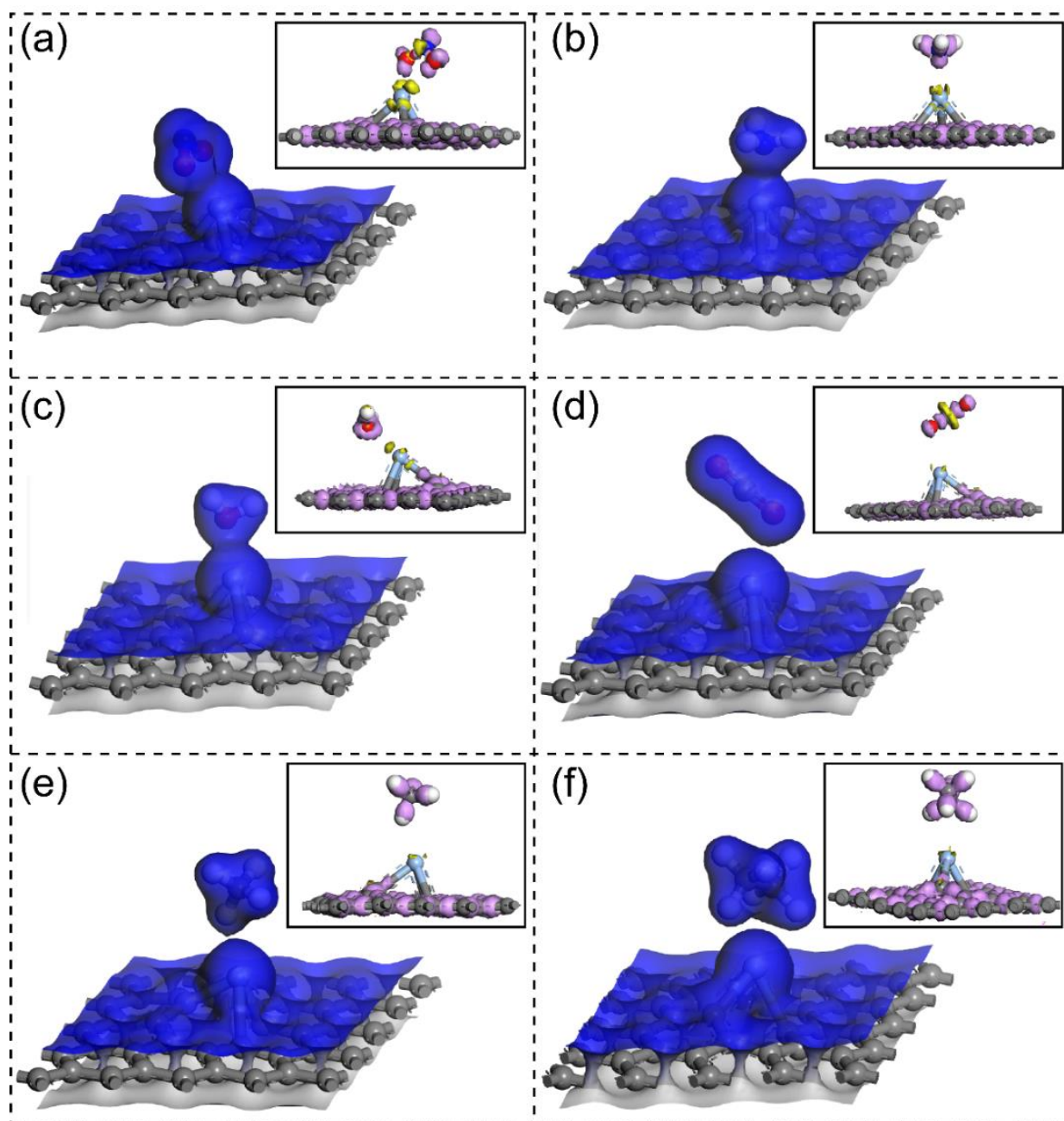


Figure 3. Total charge densities of Ag–Gr adsorption with (a) NO₂, (b) NH₃, (c) H₂O, (d) CO₂, (e) CH₄, and (f) C₂H₆; the inserts are the isosurfaces of deformation electron density with isovalues of ± 0.12 , where the yellow and pink regions represent electrons loss and accumulation, respectively.

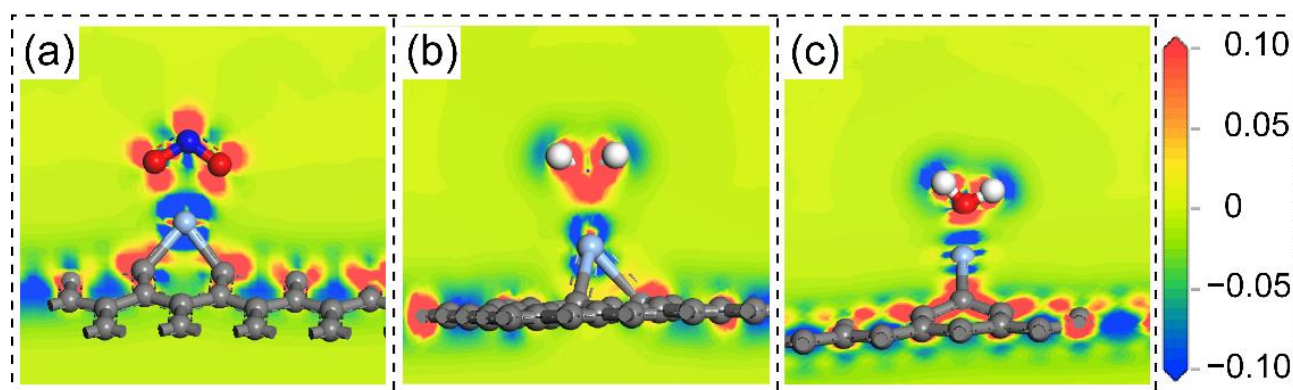


Figure 4. Difference charge densities of Ag–Gr adsorption with (a) NO₂, (b) NH₃, and (c) H₂O.

4. Conclusions and Discussions

First-principle calculations are implemented to theoretically study the gas adsorption properties on an Ag–Gr surface. The results show that the adsorption energy and Mulliken transfer charge of NO₂ adsorbed on Ag–Gr are both the largest among all tested gases. After NO₂ adsorption, the DOS changes obviously, and the total/difference charge densities illustrate a strong interaction of NO₂ and Ag–Gr. Therefore, Ag–Gr-based sensors exhibit desirable sensitivity toward NO₂. As for NH₃ and humidity, the theoretical analysis demonstrates that the interaction of these two gases with Ag–Gr is relatively weaker than that of NO₂. In addition to responding to NO₂, some experimental reports also show that graphene and its derivatives have a weak response to ammonia and water [37,51–54]. The potential interference of NH₃ and humidity can be suppressed by heating or UV illuminating the sensor. As for CO₂ and VOCs (CH₄ and C₂H₆), the small Mulliken transfer charge and no electron orbital overlap between Ag–Gr and gas molecules indicate the physisorption properties and poor sensitivity, corresponding to the good selectivity to NO₂ of Ag–Gr-based sensors. Conclusively, although there will be a minor deviation in our theoretical analysis, we still anticipate that these results will be helpful in providing instructive direction on designing future high-performance sensing materials.

Author Contributions: Conceptualization, Q.L. and Y.L.; methodology, Q.L. and Y.L.; software, Q.L. and S.D.; validation, Q.L., Y.L., D.C. (Di Chen), J.M., H.J. and D.C. (Daxiang Cui); formal analysis, Q.L.; investigation, Q.L.; resources, D.C. (Di Chen), J.M., H.J. and D.C. (Daxiang Cui); data curation, Q.L.; writing—original draft preparation, Q.L.; writing—review and editing, Q.L., Y.L., D.C. (Di Chen), J.M., X.Z., S.L., H.J. and D.C. (Daxiang Cui); supervision, D.C. (Di Chen), J.M., H.J. and D.C. (Daxiang Cui); project administration, D.C. (Di Chen), J.M., H.J. and D.C. (Daxiang Cui); funding acquisition, D.C. (Di Chen), J.M., H.J. and D.C. (Daxiang Cui) All authors have read and agreed to the published version of the manuscript.

Funding: This research was funded by National Natural Science Foundation of China (No. 61774106, 21706229 and 81971736), Science and Technology Commission of Shanghai Municipality (No. 20JC1415000, 21S31906400), and National Key Research and Development Program of China (No. 2017YFA0205301).

Institutional Review Board Statement: Not applicable.

Informed Consent Statement: Not applicable.

Data Availability Statement: Not applicable.

Acknowledgments: We are very grateful to Xiaoming Yang and Zhejiang Fulai New Materials Co., Ltd. for their great help. We acknowledge analysis support from the Instrumental Analysis Center of Shanghai Jiao Tong University.

Conflicts of Interest: The authors declare no conflict of interest.

References

1. Wang, H.; Zhou, L.; Liu, Y.; Liu, F.; Liang, X.; Liu, F.; Gao, Y.; Yan, X.; Lu, G. UV-activated ultrasensitive and fast reversible ppb NO₂ sensing based on ZnO nanorod modified by constructing interfacial electric field with In₂O₃ nanoparticles. *Sens. Actuators B Chem.* **2020**, *305*, 127498. [CrossRef]
2. Zhang, D.; Yang, Z.; Li, P.; Pang, M.; Xue, Q. Flexible self-powered high-performance ammonia sensor based on Au-decorated MoSe₂ nanoflowers driven by single layer MoS₂-flake piezoelectric nanogenerator. *Nano Energy* **2019**, *65*. [CrossRef]
3. Hu, F.-F.; Tang, H.-Y.; Tan, C.-J.; Ye, H.-Y.; Chen, X.-P.; Zhang, G.-Q. Nitrogen Dioxide Gas Sensor Based on Monolayer SnS: A First-Principle Study. *IEEE Electron Device Lett.* **2017**, *38*, 983–986. [CrossRef]
4. Wang, S.-G.; Tan, C.-J.; Yang, Q.; Xu, Y.-X.; Li, S.-L.; Chen, X.-P. A Novel Ultra-Sensitive Nitrogen Dioxide Sensor Based on Germanium Monosulfide Monolayer. *IEEE Electron Device Lett.* **2017**, *38*, 1590–1593. [CrossRef]
5. Wu, J.; Wu, Z.; Ding, H.; Wei, Y.; Huang, W.; Yang, X.; Li, Z.; Qiu, L.; Wang, X. Flexible, 3D SnS₂/Reduced graphene oxide heterostructured NO₂ sensor. *Sens. Actuators B Chem.* **2020**, *305*, 127445. [CrossRef]
6. Liao, N.; Zhou, H.; Zheng, B.; Xue, W. Silicon Oxycarbide-Derived Carbon as Potential NO₂ Gas Sensor: A First Principles' Study. *IEEE Electron Device Lett.* **2018**, *39*, 1760–1763. [CrossRef]
7. Sharma, B.; Sharma, A.; Joshi, M.; Myung, J.-h. Sputtered SnO₂/ZnO Heterostructures for Improved NO₂ Gas Sensing Properties. *Chemosensors* **2020**, *8*, 67. [CrossRef]
8. Kim, Y.; Kwon, K.C.; Kang, S.; Kim, C.; Kim, T.H.; Hong, S.-P.; Park, S.Y.; Suh, J.M.; Choi, M.-J.; Han, S.; et al. Two-Dimensional NbS₂ Gas Sensors for Selective and Reversible NO₂ Detection at Room Temperature. *ACS Sens.* **2019**, *4*, 2395–2402. [CrossRef] [PubMed]
9. Camargo Moreira, Ó.L.; Cheng, W.-Y.; Fuh, H.-R.; Chien, W.-C.; Yan, W.; Fei, H.; Xu, H.; Zhang, D.; Chen, Y.; Zhao, Y.; et al. High Selectivity Gas Sensing and Charge Transfer of SnSe₂. *ACS Sens.* **2019**, *4*, 2546–2552. [CrossRef]
10. Panigrahi, P.; Hussain, T.; Kartan, A.; Ahuja, R. Elemental Substitution of Two-Dimensional Transition Metal Dichalcogenides (MoSe₂ and MoTe₂): Implications for Enhanced Gas Sensing. *ACS Sens.* **2019**, *4*, 2646–2653. [CrossRef]
11. Meng, Z.; Stolz, R.M.; Mendecki, L.; Mirica, K.A. Electrically-Transduced Chemical Sensors Based on Two-Dimensional Nanomaterials. *Chem. Rev.* **2019**, *119*, 478–598. [CrossRef]
12. Nádherná, M.; Opekar, F.; Reiter, J. Ionic liquid–polymer electrolyte for amperometric solid-state NO₂ sensor. *Electrochim. Acta* **2011**, *56*, 5650–5655. [CrossRef]
13. Gebicki, J.; Kloskowski, A.; Chrzanowski, W.; Stepnowski, P.; Namiesnik, J. Application of Ionic Liquids in Amperometric Gas Sensors. *Crit. Rev. Anal. Chem.* **2016**, *46*, 122–138. [CrossRef] [PubMed]
14. Nádherná, M.; Opekar, F.; Reiter, J.; Štulík, K. A planar, solid-state amperometric sensor for nitrogen dioxide, employing an ionic liquid electrolyte contained in a polymeric matrix. *Sens. Actuators B Chem.* **2012**, *161*, 811–817. [CrossRef]
15. Lee, S.W.; Lee, W.; Hong, Y.; Lee, G.; Yoon, D.S. Recent advances in carbon material-based NO₂ gas sensors. *Sens. Actuators B Chem.* **2018**, *255*, 1788–1804. [CrossRef]
16. Li, Q.; Liu, Y.; Chen, D.; Miao, J.; Lin, S.; Cui, D. Highly Sensitive and Flexible Piezoresistive Pressure Sensors Based on 3D Reduced Graphene Oxide Aerogel. *IEEE Electron Device Lett.* **2021**, *42*, 589–592. [CrossRef]
17. Wu, J.; Wu, Z.; Ding, H.; Wei, Y.; Huang, W.; Yang, X.; Li, Z.; Qiu, L.; Wang, X. Three-Dimensional Graphene Hydrogel Decorated with SnO₂ for High-Performance NO₂ Sensing with Enhanced Immunity to Humidity. *ACS Appl. Mater. Interfaces* **2020**, *12*, 2634–2643. [CrossRef]
18. Niu, F.; Shao, Z.-W.; Gao, H.; Tao, L.-M.; Ding, Y. Si-doped graphene nanosheets for NO_x gas sensing. *Sens. Actuators B Chem.* **2021**, *328*. [CrossRef]
19. Huang, J.; Chen, H.; Niu, W.; Fam, D.W.H.; Palaniappan, A.; Larisika, M.; Faulkner, S.H.; Nowak, C.; Nimmo, M.A.; Liedberg, B.; et al. Highly manufacturable graphene oxide biosensor for sensitive Interleukin-6 detection. *RSC Adv.* **2015**, *5*, 39245–39251. [CrossRef]
20. Cruz-Martinez, H.; Rojas-Chavez, H.; Montejó-Alvaró, F.; Pena-Castaneda, Y.A.; Matadamas-Ortiz, P.T.; Medina, D.I. Recent Developments in Graphene-Based Toxic Gas Sensors: A Theoretical Overview. *Sensors* **2021**, *21*, 1992. [CrossRef]
21. Leenaerts, O.; Partoens, B.; Peeters, F.M. Adsorption of H₂O, NH₃, CO, NO₂, and NO on graphene: A first-principles study. *Phys. Rev. B* **2008**, *77*. [CrossRef]
22. Zhang, D.; Sun, Y.e.; Jiang, C.; Yao, Y.; Wang, D.; Zhang, Y. Room-temperature highly sensitive CO gas sensor based on Ag-loaded zinc oxide/molybdenum disulfide ternary nanocomposite and its sensing properties. *Sens. Actuators B Chem.* **2017**, *253*, 1120–1128. [CrossRef]
23. Zhang, X.; Yu, L.; Wu, X.; Hu, W. Experimental Sensing and Density Functional Theory Study of H₂S and SO₂ Adsorption on Au-Modified Graphene. *Adv. Sci.* **2015**, *2*, 1500101. [CrossRef] [PubMed]
24. Zhang, X.; Yu, L.; Gui, Y.; Hu, W. First-principles study of SF₆ decomposed gas adsorbed on Au-decorated graphene. *Appl. Surf. Sci.* **2016**, *367*, 259–269. [CrossRef]
25. Manna, B.; Chakrabarti, I.; Guha, P.K. Platinum Nanoparticles Decorated Graphene Oxide Based Resistive Device for Enhanced Formaldehyde Sensing: First-Principle Study and its Experimental Correlation. *IEEE Trans. Electron Devices* **2019**, *66*, 1942–1949. [CrossRef]
26. Gao, X.; Zhou, Q.; Wang, J.; Xu, L.; Zeng, W. Adsorption of SO₂ molecule on Ni-doped and Pd-doped graphene based on first-principle study. *Appl. Surf. Sci.* **2020**, *517*, 146180. [CrossRef]

27. Zhao, C.; Wu, H. A first-principles study on the interaction of biogas with noble metal (Rh, Pt, Pd) decorated nitrogen doped graphene as a gas sensor: A DFT study. *Appl. Surf. Sci.* **2018**, *435*, 1199–1212. [[CrossRef](#)]
28. Li, Q.; Chen, D.; Miao, J.; Lin, S.; Yu, Z.; Han, Y.; Yang, Z.; Zhi, X.; Cui, D.; An, Z. Ag-Modified 3D Reduced Graphene Oxide Aerogel-Based Sensor with an Embedded Microheater for a Fast Response and High-Sensitive Detection of NO₂. *ACS Appl. Mater. Interfaces* **2020**, *12*, 25243–25252. [[CrossRef](#)] [[PubMed](#)]
29. Makoś-Chełstowska, P.; Stupek, E.; Gębicki, J. Deep eutectic solvent-based green absorbents for the effective removal of volatile organochlorine compounds from biogas. *Green Chem.* **2021**, *23*, 4814–4827. [[CrossRef](#)]
30. Makoś, P.; Stupek, E.; Gębicki, J. Extractive detoxification of feedstocks for the production of biofuels using new hydrophobic deep eutectic solvents—Experimental and theoretical studies. *J. Mol. Liq.* **2020**, *308*. [[CrossRef](#)]
31. Gutierrez, A.; Atilhan, M.; Aparicio, S. A theoretical study on lidocaine solubility in deep eutectic solvents. *Phys. Chem. Chem. Phys.* **2018**, *20*, 27464–27473. [[CrossRef](#)]
32. Atilhan, M.; Altamash, T.; Aparicio, S. Quantum Chemistry Insight into the Interactions Between Deep Eutectic Solvents and SO₂. *Molecules* **2019**, *24*, 2963. [[CrossRef](#)]
33. Choi, S.-J.; Lee, D.-M.; Yu, H.; Jang, J.-S.; Kim, M.-H.; Kang, J.-Y.; Jeong, H.S.; Kim, I.-D. All-carbon fiber-based chemical sensor: Improved reversible NO₂ reaction kinetics. *Sens. Actuators B Chem.* **2019**, *290*, 293–301. [[CrossRef](#)]
34. Paul, R.K.; Badhulika, S.; Saucedo, N.M.; Mulchandani, A. Graphene nanomesh as highly sensitive chemiresistor gas sensor. *Anal. Chem.* **2012**, *84*, 8171–8178. [[CrossRef](#)] [[PubMed](#)]
35. Wu, J.; Tao, K.; Miao, J.; Norford, L.K. Improved Selectivity and Sensitivity of Gas Sensing Using a 3D Reduced Graphene Oxide Hydrogel with an Integrated Microheater. *ACS Appl. Mater. Interfaces* **2015**, *7*, 27502–27510. [[CrossRef](#)] [[PubMed](#)]
36. Piloto, C.; Notarianni, M.; Shafiei, M.; Taran, E.; Galpaya, D.; Yan, C.; Motta, N. Highly NO₂ sensitive caesium doped graphene oxide conductometric sensors. *Beilstein J. Nanotechnol.* **2014**, *5*, 1073–1081. [[CrossRef](#)] [[PubMed](#)]
37. Cho, B.; Yoon, J.; Hahm, M.G.; Kim, D.-H.; Kim, A.R.; Kahng, Y.H.; Park, S.-W.; Lee, Y.-J.; Park, S.-G.; Kwon, J.-D.; et al. Graphene-based gas sensor: Metal decoration effect and application to a flexible device. *J. Mater. Chem. C* **2014**, *2*, 5280–5285. [[CrossRef](#)]
38. Zhang, H.; Li, Q.; Huang, J.; Du, Y.; Ruan, S.C. Reduced Graphene Oxide/Au Nanocomposite for NO(2) Sensing at Low Operating Temperature. *Sensors* **2016**, *16*, 1152. [[CrossRef](#)]
39. Wu, J.; Wu, Z.; Ding, H.; Yang, X.; Wei, Y.; Xiao, M.; Yang, Z.; Yang, B.R.; Liu, C.; Lu, X.; et al. Three-Dimensional-Structured Boron- and Nitrogen-Doped Graphene Hydrogel Enabling High-Sensitivity NO₂ Detection at Room Temperature. *ACS Sens.* **2019**, *4*, 1889–1898. [[CrossRef](#)]
40. Li, L.; He, S.; Liu, M.; Zhang, C.; Chen, W. Three-dimensional mesoporous graphene aerogel-supported SnO₂ nanocrystals for high-performance NO₂ gas sensing at low temperature. *Anal. Chem.* **2015**, *87*, 1638–1645. [[CrossRef](#)]
41. Zhang, B.; Cheng, M.; Liu, G.; Gao, Y.; Zhao, L.; Li, S.; Wang, Y.; Liu, F.; Liang, X.; Zhang, T.; et al. Room temperature NO₂ gas sensor based on porous Co₃O₄ slices/reduced graphene oxide hybrid. *Sens. Actuators B Chem.* **2018**, *263*, 387–399. [[CrossRef](#)]
42. Cho, B.; Yoon, J.; Lim, S.K.; Kim, A.R.; Kim, D.H.; Park, S.G.; Kwon, J.D.; Lee, Y.J.; Lee, K.H.; Lee, B.H.; et al. Chemical Sensing of 2D Graphene/MoS₂ Heterostructure device. *ACS Appl. Mater. Interfaces* **2015**, *7*, 16775–16780. [[CrossRef](#)] [[PubMed](#)]
43. Kumar, J.; Nemade, H.B.; Giri, P.K. Adsorption of Small Molecules on Niobium Doped Graphene: A Study Based on Density Functional Theory. *IEEE Electron Device Lett.* **2018**, *39*, 296–299. [[CrossRef](#)]
44. Cui, H.; Zheng, K.; Zhang, Y.; Ye, H.; Chen, X. Superior Selectivity and Sensitivity of C₃N Sensor in Probing Toxic Gases NO₂ and SO₂. *IEEE Electron Device Lett.* **2018**, *39*, 284–287. [[CrossRef](#)]
45. Zhang, D.; Cao, Y.; Yang, Z.; Wu, J. Nanoheterostructure Construction and DFT Study of Ni-Doped In₂O₃ Nanocubes/WS₂ Hexagon Nanosheets for Formaldehyde Sensing at Room Temperature. *ACS Appl. Mater. Interfaces* **2020**, *12*, 11979–11989. [[CrossRef](#)] [[PubMed](#)]
46. Li, Q.; Chen, D.; Miao, J.; Lin, S.; Yu, Z.; Cui, D.; Yang, Z.; Chen, X. Highly sensitive sensor based on ordered porous ZnO nanosheets for ethanol detecting application. *Sens. Actuators B Chem.* **2021**, *326*. [[CrossRef](#)]
47. Luo, H.-C.; Meng, R.-S.; Gao, H.L.; Sun, X.; Xiao, J.; Ye, H.-Y.; Zhang, G.-Q.; Chen, X.-P. First-Principles Study of Nitric Oxide Sensor Based on Blue Phosphorus Monolayer. *IEEE Electron Device Lett.* **2017**, *38*, 1139–1142. [[CrossRef](#)]
48. Jin, C.; Tang, X.; Tan, X.; Smith, S.C.; Dai, Y.; Kou, L. A Janus MoSSe monolayer: A superior and strain-sensitive gas sensing material. *J. Mater. Chem. A* **2019**, *7*, 1099–1106. [[CrossRef](#)]
49. Tang, X.; Shang, J.; Gu, Y.; Du, A.; Kou, L. Reversible gas capture using a ferroelectric switch and 2D molecule multiferroics on the In₂Se₃ monolayer. *J. Mater. Chem. A* **2020**, *8*, 7331–7338. [[CrossRef](#)]
50. Wu, J.; Wei, Y.; Ding, H.; Wu, Z.; Yang, X.; Li, Z.; Huang, W.; Xie, X.; Tao, K.; Wang, X. Green Synthesis of 3D Chemically Functionalized Graphene Hydrogel for High-Performance NH₃ and NO₂ Detection at Room Temperature. *ACS Appl. Mater. Interfaces* **2020**, *12*, 20623–20632. [[CrossRef](#)]
51. Tian, W.; Liu, X.; Yu, W. Research Progress of Gas Sensor Based on Graphene and Its Derivatives: A Review. *Appl. Sci.* **2018**, *8*, 1118. [[CrossRef](#)]
52. Donarelli, M.; Ottaviano, L. 2D Materials for Gas Sensing Applications: A Review on Graphene Oxide, MoS(2), WS(2) and Phosphorene. *Sensors* **2018**, *18*, 3638. [[CrossRef](#)] [[PubMed](#)]

-
53. Li, H.; Wu, J.; Qi, X.; He, Q.; Liusman, C.; Lu, G.; Zhou, X.; Zhang, H. Graphene oxide scrolls on hydrophobic substrates fabricated by molecular combing and their application in gas sensing. *Small* **2013**, *9*, 382–386. [[CrossRef](#)] [[PubMed](#)]
 54. Borini, S.; White, R.; Wei, D.; Astley, M.; Haque, S.; Spigone, E.; Harris, N.; Kivioja, J.; Ryhanen, T. Ultrafast Graphene Oxide Humidity Sensors. *ACS Nano* **2013**, *7*, 11166–11173. [[CrossRef](#)] [[PubMed](#)]